Shahid Chamran
University of Ahvaz

Journal of

Applied and Computational Mechanics

Research Paper

The Effect of Magneto-hydrodynamics on Curved Circular Plate and Porous-rough Flat Plate with Non-Newtonian Fluid

J. Jayaprakash[1] , Vediyappan Govindan[1] , Jagadish Patil[2] , Bannihalli N. Hanumagowda[3] ,
Hijaz Ahmad[4,5,6,7] , Jagadish V. Tawade[8]

[1] Department of Mathematics, Hindustan Institute of Technology and Science, Chennai, India

[2] Department of Mathematics, Faculty of Engineering and Technology, Sharnbasva University, Kalaburagi, India

[3] Department of Mathematics, School of Applied Sciences, REVA University, Bangalore, Karnataka, India

[4] Department of Mathematics, Faculty of Science, Islamic University of Madinah, Medina, Saudi Arabia

[5] Near East University, Operational Research Center in Healthcare, TRNC Mersin 10, Nicosia, 99138, Turkey

[6] Center for Applied Mathematics and Bioinformatics, Gulf University for Science and Technology, Kuwait

[7] Department of Computer Science and Mathematics, Lebanese American University, Beirut, Lebanon

[8] Department of Mathematics, Vishwakarma University, Pune-411048, India

Abstract. This study explores the effect of theoretical MHD on curved circular and flat plates using non-Newtonian lubricant. Lower flat plate is porous and rough. The Stokes theory has been used to incorporate the couple stress effects. Furthermore, Darcy law is taken into account for porous medium. Average pressure, load support and squeeze film time are determined from Christensen theory. The numerical results for bearing characteristics such as pressure, load carrying capacity and squeeze film time are plotted graphically to study the influence of curved circular and flat plate. This investigation shows that the squeeze film characteristics are higher in azimuthal roughness patterns and lower in radial patterns due to roughness parameter. In addition, MHD and couple stress boost the pressure, load support and squeezing time compared to Newtonian and non-magnetic cases. The effect of permeability of the porous layer is to decrease the load carrying capacity as it gives an easy path for the lubricant to pass through.

Keywords: Magnetohydrodynamic, Squeeze film, Curved circular plate, Porous flat plate.

1. Introduction

Recently, many engineering and industrial applications have highlighted magnetohydrodynamics (MHD) in flow analysis. MHD bearings with conducting fluids have better electrical and thermal conductivity than conventional bearings. The usage of non-Newtonian fluids has increased with machine tool technology. New research reveals that adding long-chained additives to base oil enhances its lubricating capabilities, reducing friction and interface damage. Numerous models from micro continuum theory have been employed to examine non-Newtonian fluid rheology.

Considering surface roughness is now an important part of engineering studies and practical applications. Bearings make use of surface roughness measurements, which indicate the degree to which a surface changes in texture. Coefficients of friction are greater on rough surfaces compared to smooth ones. Bearings with porous surfaces do not require external lubrication over the entire lifespan of the machine since the pores in that area are filled with oil. Hydrodynamic oil film generation is caused by the injection of oil into a porous matrix at a rate proportional to the journal movement speed. Researchers have conducted a plethora of experimental studies on porous bearing performance during the past few decades. Short journal bearings can be solved using the Darcy model, which was proposed by Morgan and Cameron in their theory of hydrodynamic porous journal bearings. Drawing on this work, a large number of researchers have studied oil bearing lubrication properties using the Darcy equation.

Morgan [1] analyzed the hydrodynamic lubrication porous metal bearings. Couple stress effects on double layered porous slider bearing studied by Buzurke et al. [2]. Bhat [3] and Bhat and Daheri [4], Rouleau [5] described the narrow press-fitted porous metal bearings bearing with hydrodynamic lubrication. MHD non-Newtonian of porous wide slider bearing was analyzed by Hanumagowda and Kashinath [6], the various physical significance of porous bearings in presence of MHD and couple stress have been studied by Naduvinamani et al. [7], Bartz and Ehlert [08] and Biradar [09], Srinivasacharya et al. [10] described the couple stress fluid between two parallel porous plates, in this study clearly explained the impacts of couple stress and Reynolds

number on velocity and temperature profile. Salma et al. [11] worked on curved circular and flat plate with viscosity variation, from this analysis squeeze film properties are enhanced by lubricating with a non-Newtonian fluid and applying a magnetic force. The squeeze film properties are improved when viscosity varies compared to a constant viscosity, and pressure, load bearing capacity, and response time are reduced when permeability is considered in contrast to a non-porous scenario. Vivek kumar et al. [12] described the study on porous thrust bearing. Out frame of this work illustrates under existence of porous parameter and magnetic field, utilise a circular pocket to improve steady-state performance metrics. Better rotor-dynamic performance is a design criterion for the bearing, thus elliptical and annular pockets are better. Shalini and Vinay [13] framed the analysis on porous journal bearings. Revealed form this study the actions of the couple-stress fluid contribute to the increased pressure distribution that occurs inside the fluids structure. It takes longer for the skin to come into contact with each other because greater weight bearing capacity and delayed squeezing time both and lessen the amount of skin friction. Naduvinamani and Rakesh [14] studied porous Rayleigh step slider bearings. This study demonstrates the porous layer's load-bearing capability is diminished because lubricant passes through easily. Using two layers of porous face with different permeabilities can reduce this impact. The load carrying capacity and coefficient of friction of double-layered porous bearings are higher than those of single-layered ones. Sampathkumar and Pai [15] worked out on porous circular bearing with Casson fluids. Biplab et al. [16] described the concept of micro polar fluid effect on porous hydrostatic journals. It revealed that, in comparison to conventional hydrostatic bearings, the one under investigation has a load-carrying capacity that is 75% higher and a static stiffness that is 80% higher. Compared to other types of hydrostatic bearings, the porous hydrostatic journal bearing has a more cost-effective performance because it has a lower flow rate and pump power need of 40% and it produces 50 % less heat.

The computation of the interaction between real objects and their environments relies significantly on roughness properties. A rough surface often has a greater coefficient of friction and wears down more rapidly than a smooth one. The production cost goes up when roughness goes down. Christensen [17] introduced the theory of stochastic model hydrodynamic lubrication of surface roughness of the bearings. Many researchers used this theory to study the performance of surface roughness on the bearing systems with MHD and couple stress. Buzurke et al. [18] elaborates the roughness effects on rectangular plates with MHD and couple stress, the author noted that the roughness parameter, magnetic field & couple stress lubricant boost the pressure and load support capacity. Davies [19], Prajapati [20], Ting [21], Vadher et al. [22], and Rajshekhar and Kashinath [23] described the behavior of bearing systems with roughness of MHD and non-Newtonian lubricants. Recently, numerous authors have made a study on different bearings [24-28]. From the Amit Kumar study, the results of this study show that radial (azimuthal) roughness patterns are affected by surface roughness and porosity, and that response time and load-capacity are both affected by the viscosity variation of Rabinowitsch fluid, in comparison to non-porous, smooth surfaces and the isoviscous case.

After the rigorous literature survey, the author observed that there has been a notable gap in research concerning the impacts of Magnetohydrodynamic (MHD) couple stress on both flat and curved circular plates incorporating porous surface roughness. Therefore, this study aims to address this gap by presenting a comprehensive theoretical examination of the effects of MHD on flat plates containing both porous-rough flat plates, as well as on curved circular plates immersed in fluids exhibiting couple stress characteristics. Through meticulous analysis and exploration, this research endeavours to shed light on MHD phenomena and the specific attributes of porous media and surface roughness, thereby contributing to a deeper understanding of the complex dynamics governing these systems.

2. Mathematical Solution

Figure 1 shows the squeeze film mechanism between a curved circular and fat plate. A uniform squeeze film is considered from the upper plate towards the bottom porous-rough fat plate at $(V = -\partial h_m / \partial t)$. It is assumed that the system lubricant is electrically conductive and isothermal. A uniform transverse magnetic field B_0 is applied in z-direction. Consider a thin fluid layer with low inertia, negligible body force except for Lorentz force and small induced magnetic field compared to the applied magnetic field. The film thickness is considered to have two parts as follows:

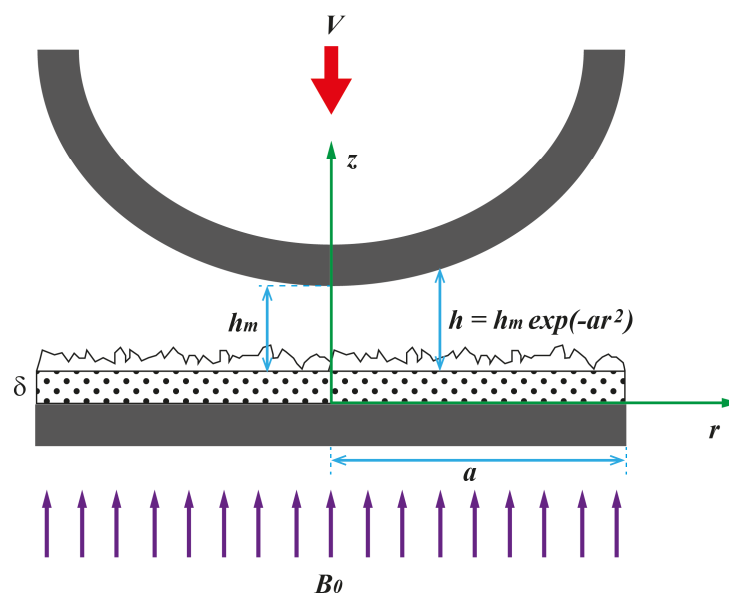$$H = h + h_s(r,z,\xi) \tag{1}$$

Fig. 1. Geometry of porous-rough flat and curved circular plates.

where $h = h_m \exp(-a^2 r), 0 \leq r \leq a$ denotes the thickness for smooth part and $h_s(r,z,\xi)$ is the rough structure, h_m is the minimum thickness, following these assumptions, the basic governing equations are:

$$\mu \frac{\partial^2 u}{\partial z^2} - \eta \frac{\partial^4 u}{\partial z^4} - \sigma B_0^2 u = \frac{\partial p}{\partial r} \tag{2}$$

$$\frac{\partial p}{\partial z} = 0 \tag{3}$$

$$\frac{1}{r} \frac{\partial}{\partial r}(ru) + \frac{\partial w}{\partial z} = 0 \tag{4}$$

where u, v are the components of velocity in r and θ directions, respectively, P denotes the pressure of film region, η is new material constant for couple stress, μ is the dynamic viscosity and σ represents the electrical conductivity.

For the porous region, we have:

$$\frac{1}{r} \frac{\partial(ru^*)}{\partial r} + \frac{\partial w^*}{\partial z} = 0 \tag{5}$$

where the components of velocities u^* and w^* in the porous matrix from the Darcy's law are given by:

$$u^* = \frac{-k}{\mu\left(1 - \phi + \dfrac{kM^2}{mh_m^2}\right)} \frac{\partial p^*}{\partial r} \tag{6}$$

$$w^* = \frac{-k}{\mu(1-\phi)} \frac{\partial p^*}{\partial z} \tag{7}$$

where $\phi = (\eta/\mu)/k$ is the ratio of microstructure size to pore size, m is porosity and k denotes the permeability porous material. The relevant conditions for components of velocity are as follows:

i) At the lower plate z = 0

$$u = 0, \quad \frac{\partial^2 u}{\partial z^2} = 0 \tag{8a}$$

$$w = 0 \tag{8b}$$

ii) At the upper plate z = H

$$u = 0, \quad \frac{\partial^2 u}{\partial z^2} = 0 \tag{9a}$$

$$w = V = -\partial h_m / \partial t \tag{9b}$$

The velocity u can be obtained by solving Eq. (2) and considering Eqs. (8a) and (9a) as follows:

$$u = \left\{(g_1 - g_2) - 1\right\} \frac{h_m^2}{\mu M^2} \frac{\partial p}{\partial r} \tag{10}$$

where $l = (\eta/\mu)^{1/2}$ is the couple stress parameter and $M = B_0 h_m (\sigma/\mu)^{1/2}$ is the Hartmann number.

$$g_1 = g_{11}, \quad g_2 = g_{12} \quad \text{for} \quad 4M^2 l^2/h_m^2 < 1 \tag{11a}$$

$$g_1 = g_{21}, \quad g_2 = g_{22} \quad \text{for} \quad 4M^2 l^2/h_m^2 = 1 \tag{11b}$$

$$g_1 = g_{31}, \quad g_2 = g_{32} \quad \text{for} \quad 4M^2 l^2/h_m^2 > 1 \tag{11c}$$

Appendix A contains the corresponding relations for Eqs. (11a), (11b) and (11c). Integrating Eq. (4) in the polar form and using conditions (8b) and (9b), one gets the Reynolds equation as:

$$\frac{1}{r\mu} \frac{\partial}{\partial r}\left\{rS(h,l,M)\frac{\partial p}{\partial r}\right\} = w_h - w_0 \tag{12}$$

Here upper plate is non-porous $w_h = 0$.

The component of velocity in z direction is continuous in interface between the lower plate, one obtains:

$$w_0 = -\left\{ \frac{dh}{dt} + \frac{k}{\mu(1-\phi)} \left(\frac{\partial p^*}{\partial z} \right)_{z=0} \right\} \tag{13}$$

Substituting Eq. (13) in Eq. (12), one gets the modified form of Reynolds equation as follows:

$$\frac{1}{r\mu} \frac{\partial}{\partial r} \left\{ rS(h,l,M) \frac{\partial p}{\partial r} \right\} = \frac{dh}{dt} + \frac{k}{\mu(1-\phi)} \left(\frac{\partial p^*}{\partial z} \right)_{z=0} \tag{14}$$

where

$$S(h,l,M) = \begin{cases} \dfrac{h_m^2}{M^2} \left\{ \dfrac{2l}{(A^2-B^2)} \left(\dfrac{B^2}{A} \tanh \dfrac{Ah}{2l} - \dfrac{A^2}{B} \tanh \dfrac{Bh}{2l} \right) + h \right\}, & \text{for } M^2 l^2 / h_m^2 < 1 \\[3mm] \dfrac{h_m^2}{M^2} \left\{ \dfrac{h}{2} \operatorname{sech}^2 \left(\dfrac{h}{2\sqrt{2l}} \right) - 3\sqrt{2l} \tanh \left(\dfrac{h}{2\sqrt{2l}} \right) + h \right\}, & \text{for } M^2 l^2 / h_m^2 = 1 \\[3mm] \dfrac{h_m^2}{M^2} \left\{ \dfrac{2lh_m}{M} \left(\dfrac{(\cot\theta A_2 - B_2)\sin B_2 h - (B_2 \cot\theta + A_2)\sin A_2 h}{\cos B_2 h + \cosh A_2 h} \right) + h \right\}, & \text{for } M^2 l^2 / h_m^2 > 1 \end{cases}$$

Integrating Eq. (14) w.r.t z over porous thickness δ and using $\partial p^* / \partial r = 0$ at $z = -\delta$ results in:

$$\left(\frac{\partial p^*}{\partial z} \right)_{z=0} = -\left(\frac{1-\phi}{D} \right) \int_{-\delta}^{0} \frac{1}{r} \frac{\partial}{\partial r} \left(r \frac{\partial p^*}{\partial r} \right) dz \tag{15}$$

Assuming that δ is very small and considering the pressure condition $p = p^*$ at porous interface $z = 0$, one obtains:

$$\left(\frac{\partial p^*}{\partial z} \right)_{z=0} = -\delta \left(\frac{1-\phi}{D} \right) \frac{1}{r} \frac{\partial}{\partial r} \left(r \frac{\partial p}{\partial r} \right) \tag{16}$$

Using Eq. (16) in Eq. (14) leads to:

$$\frac{1}{r} \frac{\partial}{\partial r} \left\{ \left(S(h,l,M) + \frac{\delta k}{D} \right) r \frac{\partial p}{\partial r} \right\} = V\mu \tag{17}$$

The above Reynolds equation describes the MHD porous influence in the fluid film region. In order to examine how surface roughness affects the performance of the system, we use the stochastic mean Reynolds from Eq. (17):

$$\frac{1}{r} \frac{\partial}{\partial r} \left\{ E \left(S(h,l,M) + \frac{\delta k}{D} \right) r \frac{\partial E(p)}{\partial r} \right\} = V\mu \tag{18}$$

where

$$E(\bullet) = \int_{-\infty}^{\infty} (\bullet) f(h_s) dh_s \tag{19}$$

The probability distribution function $f(h_s)$ for the stochastic film thickness can be defined as:

$$f(h_s) = \begin{cases} \dfrac{35}{32c^7} (c^2 - h_s^2)^3, & -c < h_s < c \\[2mm] 0, & \text{elsewhere} \end{cases}$$

where h_s is the stochastic film thickness, $\bar{\sigma}$ is the standard deviation and $c = 3\bar{\sigma}$.

- **Radial roughness Pattern**

For 1D radial roughness structures, the surface roughness takes the form of long, thin ridges and valleys running in r-direction and the film thickness is given by:

$$H = h + h_s(z, \xi) \tag{20}$$

Then Eq. (18) becomes:

$$\frac{1}{r} \frac{\partial}{\partial r} \left\{ E \left(S(h,l,M) + \frac{\delta k}{D} \right) r \frac{\partial E(p)}{\partial r} \right\} = \mu V \tag{21}$$

- **Azimuthal roughness Pattern**

In 1D Azimuthal roughness pattern, the surface roughness is depicted by long, narrow ridges and valleys flowing in z-direction and overall film thickness is given by:

$$H = h + h_s(r, \xi) \tag{22}$$

Then Eq. (18) becomes:

$$\frac{1}{r} \frac{\partial}{\partial r} \left\{ \left[\frac{1}{E\left(\frac{1}{S(h,l,M)}\right)} + \frac{\delta k}{D} \right] r \frac{\partial E(p)}{\partial r} \right\} = V\mu \tag{23}$$

From Eqs. (21) and (23), we have:

$$\frac{1}{r} \frac{\partial}{\partial r} \left\{ \left(K(H,l,M,c) + \frac{\delta k}{D} \right) r \frac{\partial E(p)}{\partial r} \right\} = V\mu \tag{24}$$

where

$$K(H,l,M,c) = \begin{cases} E(S(H,l,M)), & \text{for Radial Roughness} \\ E\left(\frac{1}{S(H,l,M)} \right), & \text{for Azimuthal Roughness} \end{cases}$$

Introducing below dimensionless parameters:

$$r^* = \frac{r}{a}, H^* = \frac{H}{h_m}, l^* = \frac{2l}{h_m}, P^* = -\frac{h_m^3 E(p)}{\mu a^2 V}, C = \frac{c}{h_m}, \delta^* = \frac{\delta}{h_0}, \psi = \frac{k\delta}{h_0^3}, D_1 = \left(1 - \phi + \frac{\psi M^2}{m\delta^*} \right)$$

and using above parameters in Eq. (24), one obtains the modified Reynolds equation as follows:

$$\frac{1}{r^*} \frac{\partial}{\partial r^*} \left[\left\{ G^*(H^*, l^*, M, C) + \frac{\psi}{D_1} \right\} r^* \frac{\partial P^*}{\partial r^*} \right] = 1 \tag{25a}$$

$$G^*(H^*, l^*, M, C) = \begin{cases} E\left\{ K^*(H^*, l^*, M) \right\}, & \text{for Radial Roughness} \\ E\left(\frac{1}{K^*(H^*, l^*, M)} \right), & \text{for Azimuthal Roughness} \end{cases} \tag{25b}$$

$$K^*(H^*, l^*, M) = \begin{cases} \frac{h_m^2}{M^2} \left\{ \frac{l^*}{(A^{*2} - B^{*2})} \left(\frac{B^{*2}}{A^*} \tanh \frac{A^* H^*}{l^*} - \frac{A^{*2}}{B^*} \tanh \frac{B^* H^*}{l^*} \right) + H^* \right\} & \text{for } M^2 l^{*2} < 1 \\ \frac{h_m^2}{M^2} \left\{ \frac{H^*}{2} \operatorname{sech}^2 \left(\frac{H^*}{\sqrt{2l^*}} \right) - \frac{3l^*}{\sqrt{2}} \tanh \left(\frac{H^*}{\sqrt{2l^*}} \right) + H^* \right\}, & \text{for } M^2 l^{*2} = 1 \\ \frac{h_m^2}{M^2} \left\{ \left(\frac{l^* \left(A_2^* \cot \theta^* - B_2^* \right) \sin B_2^* H^* - l^* \left(B_2^* \cot \theta^* + A_2^* \right) \sinh A_2^* H^*}{M_0 (\cos B_2^* H^* + \cosh A_2^* H^*)} \right) + H^* \right\} & \text{for } M^2 l^{*2} > 1 \end{cases} \tag{25c}$$

$$A^* = \left(\frac{1 + \left(1 - l^{*2} M^2\right)^{1/2}}{2} \right)^{1/2} \text{ and } B^* = \left(\frac{1 - \left(1 - l^{*2} M^2\right)^{1/2}}{2} \right)^{1/2} \tag{25d}$$

Integrating Eq. (25a) w.r.t r^* and using the boundary conditions:

$$\frac{\partial P^*}{\partial r^*} = 0 \text{ at } r^* = 0 \text{ and } P^* = 0 \text{ at } r^* = 1 \tag{26a}$$

$$P^* = -\frac{1}{2} \int_1^{r^*} \frac{r^*}{G^*(H^*, l^*, M, C) + \frac{\psi}{D_1}} dr^* \tag{26b}$$

results in the non-dimensional pressure P^* defined in Eq. (26b).

By integrating Eq. (26b) exerted on curved circular plate, mean load support capacity is given by:

$$W^* = \frac{h_m^3 E(w)}{\mu a^2 V} = -\frac{1}{2} \int_0^1 \left\{ \int_1^{r^*} \frac{r^*}{G^*(H^*, l^*, M, C) + \frac{\psi}{D_1}} dr^* \right\} r^* dr^* \tag{27}$$

The Squeeze film time relation in non-dimensional representation is expressed as:

$$T^* = -\frac{1}{2}\int_1^{h^*}\left[\int_0^1\left\{\int_1^{r^*}\frac{r^*}{G^*(H^*,l^*,M,C)+\frac{\psi}{D_1}}dr^*\right\}r^*dr^*\right]dh_m^*$$

(28)

3. Results and Discussions

In current the study, the influence of magnetic field on non-dimensional pressure, load support and squeeze film time expression with a couple stress fluids is analyzed. The squeeze film properties are obtained as a function of the Hartmann number M_0, couple stress parameter l^*, Roughness parameter C and permeability parameter ψ. The combined study of MHD couple stress flat plate with porous-rough curved circular plate is then presented. In this analysis, the non-dimensional parameters are considered within the following ranges: $C = 0, 0.2, 0.4$, $\psi = 0, 0.001, 0.1$, $M = 0, 2, 4$, $l^* = 0, 0.2, 0.4$, and $\beta = -0.25, 0, 0.25$, keeping fixed values for $m = 0.6$, $\delta = 0.01$ and $\phi = 0.01$.

3.1. Dimensionless squeeze film pressure

Figure 2 describes P^* versus r^* for different roughness parameter C and taking into account $M = 2$, $l^* = 0.2$, $\beta = 0.5$, $m = 0.6$, $\psi = 0.001$, $\delta = 0.01$ and $\phi = 0.2$ for both roughness patterns. From this graph, it is clear that the pressure is enhanced due to the impact of roughness parameter. The elaboration of pressure in polar coordinates r^* with distinct values of ψ is displayed in Fig. 3 and noted the pressure P^* increased as ψ increases. Figures 4 and 5 examine the variation of non-dimensional P^* with axial polar coordinate r^* for several amounts of M and l^* by assuming $\beta = 0.5$, $m = 0.6$, $\psi = 0.001$, $\delta = 0.01$, $\phi = 0.2$ and $C = 0.3$. Here, we observe the larger pressure due to Hartmann number and non-Newtonian lubricant effects. We have drawn P^* against r^* for some assigned values of β in Fig. 6. It is shown that there is a rise in pressure for small values of curvature parameter β. Furthermore, it is evident that P^* increase for azimuthal pattern compared to that of radial pattern for all the cases of ψ, M, l^* and β. More magnetic fields in the lubricant enhance its interaction with the induced magnetic field. Film fluid velocity falls when a continuously applied magnetic field contains a large amount of fluid, opposed to the normal configurations. Roughness and non-Newtonian fluid keep pressure evenly distributed. Because the couple stress fluid counteracts the flowing fluid, it accumulates more fluid. However, bearing surface roughness decreases the fluid velocity. Surface asperities further limit lubricant leaking from the sides. The presence of large amounts of fluid in the area results in a high-pressure distribution. As a result, magnetic field, roughness, and non-Newtonian fluids improve the pressure distribution.
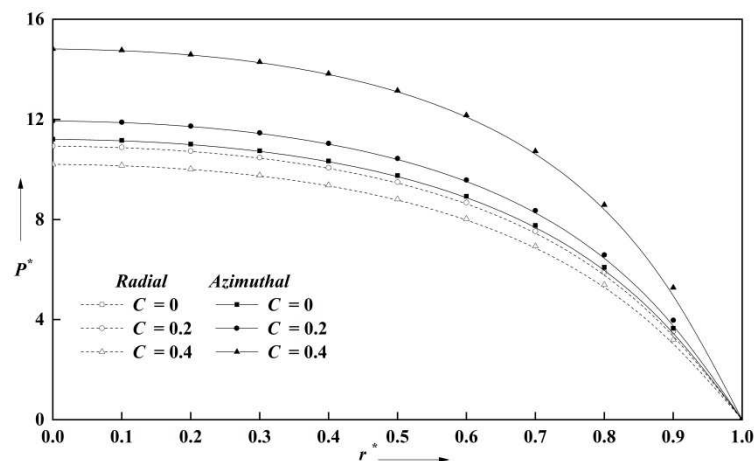

Fig. 2. Variation of non-dimensional pressure P^* with r^* for different values of C with $M = 2, l^* = 0.3, m = 0.6, \beta = 0.5, \phi = 0.2, \delta = 0.01, \psi = 0.001$.
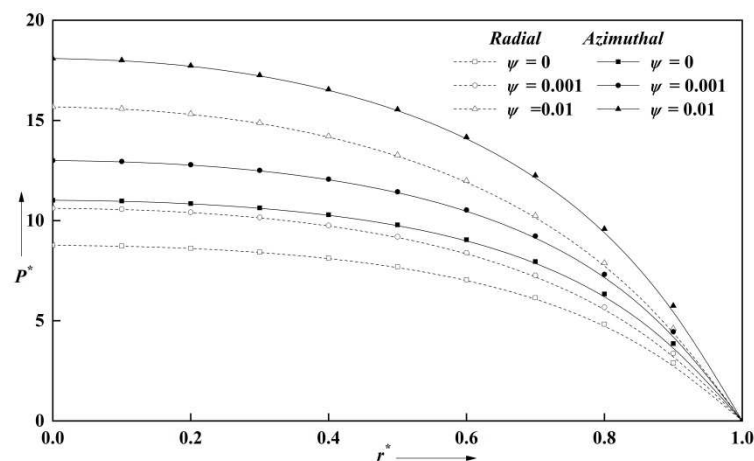

Fig. 3. Variation of non-dimensional pressure P^* with r^* for different values of ψ with $M = 2, l^* = 0.3, m = 0.6, \beta = 0.5, \phi = 0.2, \delta = 0.01, C = 0.3$.
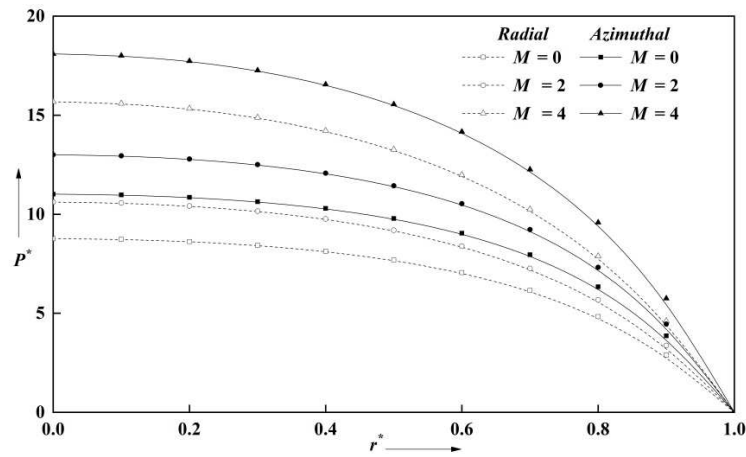
Fig. 4. Variation of non-dimensional pressure P^* with r^* for different values of M with $l^* = 0.3, m = 0.6, \beta = 0.5, \phi = 0.2, \delta = 0.01, C = 0.3, \psi = 0.001$.
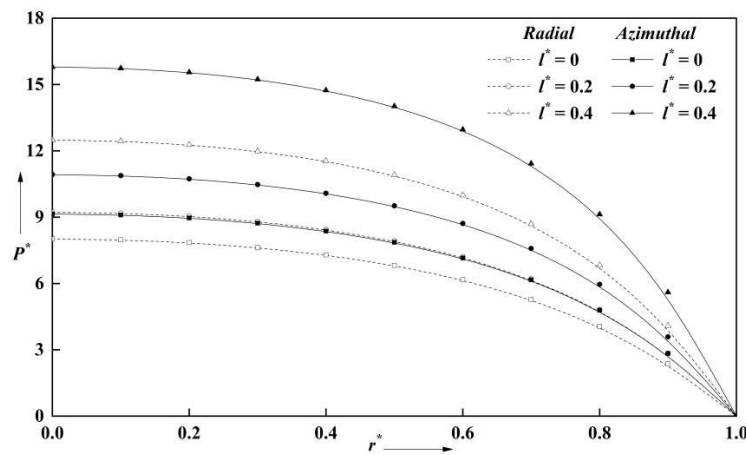

Fig. 5. Variation of non-dimensional pressure P^* with r^* for different values of l^* with $M = 2, m = 0.6, \beta = 0.5, \phi = 0.2, \delta = 0.01, C = 0.3, \psi = 0.001$.
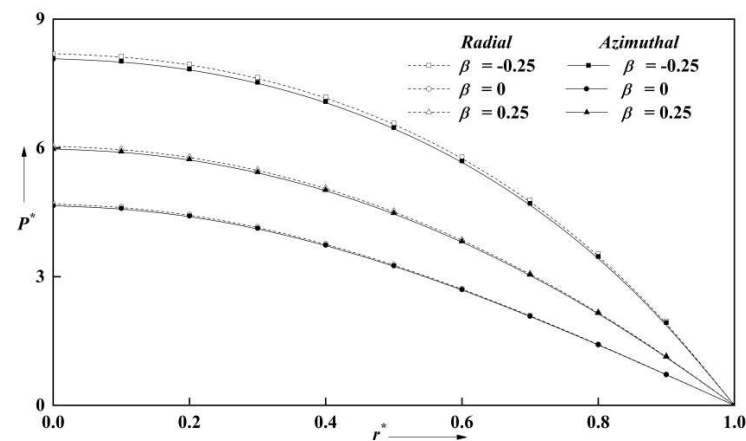

Fig. 6. Variation of non-dimensional pressure P^* with r^* for different values of β with $M = 2, m = 0.6, l^* = 0.3, \phi = 0.2, \delta = 0.01, C = 0.3, \psi = 0.001$.

3.2. Dimensionless load support capacity

The Graphs of W^* against β for distinct values of C by keeping constant other parameters as: $M = 2$, $l^* = 0.2$, $\beta = 0.5$, $m = 0.6$, $\psi = 0.001$, $\delta = 0.01$ and $\phi = 0.2$ for both roughness patterns is shown in Fig. 7. The load support capacity is significantly rises by increasing C in azimuthal structure whereas it is opposite in the radial structure. Figure 8 displays the load W^* against β for assigned values of ψ and $M = 2$, $l^* = 0.2$, $\beta = 0.5$, $m = 0.6$, $\delta = 0.01$, $\phi = 0.2$ and $C = 0.3$. It is seen that the load support is falling as the parameter ψ increases. The scientific reason behind this phenomenon is that the higher permeability parameter creates more empty space on the porous escape of the lubricant. From this result, there is no pressure rise in fluid film region so that it reduces the load carrying capacity. Figures 9 and 10 examine the variation of load W^* in terms of β for distinct Hartmann number M and l^* when the other parameters are fixed: $\beta = 0.5$, $m = 0.6$, $\delta = 0.01$, $\phi = 0.2$, $\psi = 0.001$ and $C = 0.3$. It is found that the load support is increased by increasing the magnetization and couple stress lubricant compared to the non-magnetic and Newtonian cases.
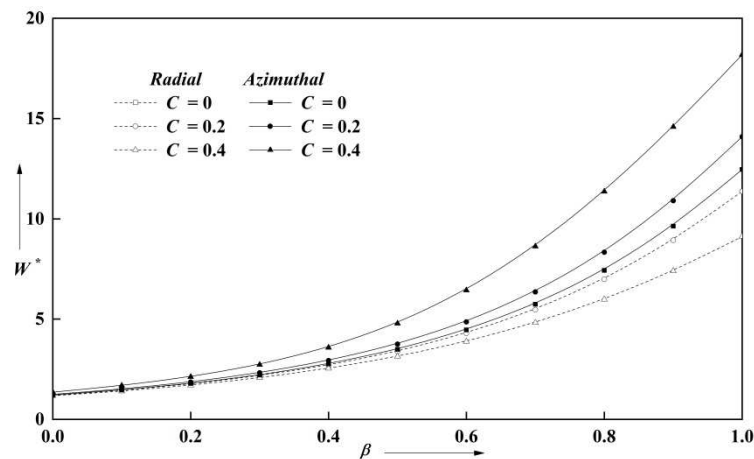
Fig. 7. Variation of non-dimensional load W^* with β for different values of C with $M = 2, m = 0.6, l^* = 0.3, \phi = 0.2, \delta = 0.01, \psi = 0.001$.
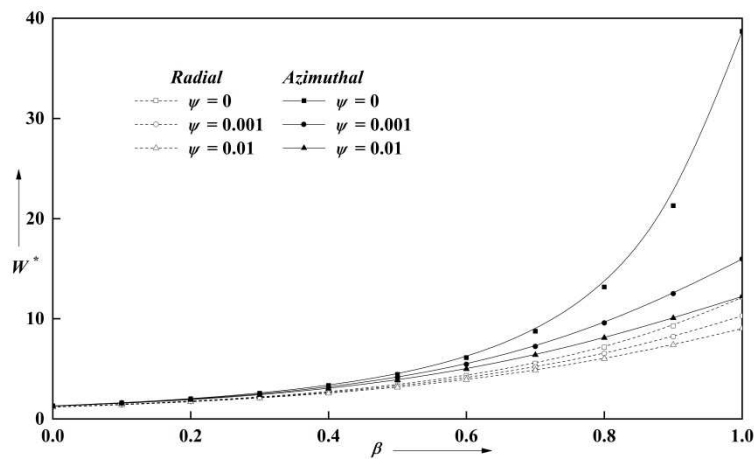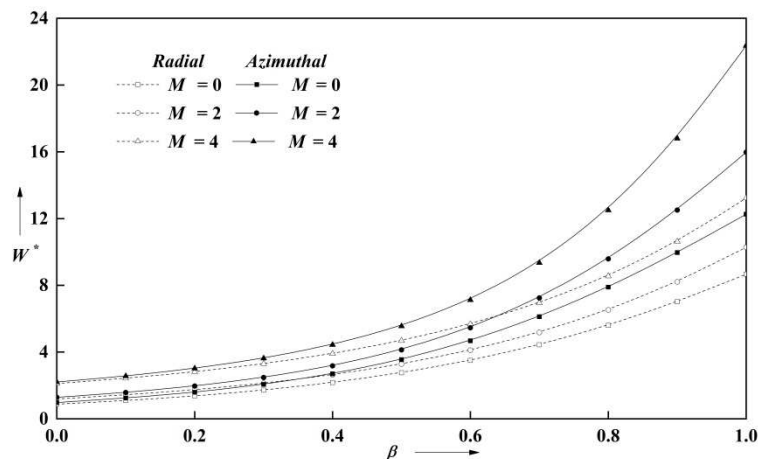

Fig. 8. Variation of non-dimensional load W^* with β for different values of ψ with $M = 2, m = 0.6, l^* = 0.3, \phi = 0.2, \delta = 0.01, C = 0.3$.

Fig. 9. Variation of non-dimensional load W^* with β for different values of M with $\psi = 0.001, m = 0.6, l^* = 0.3, \phi = 0.2, \delta = 0.01, C = 0.3$.

3.3. Non-dimensional squeeze film time

Figure 11 elaborates the squeezing time T^* versus h_m^* with distinct values of parameter C for both types of roughness patterns and taking into account that $M = 2, l^* = 0.2, \beta = 0.5, m = 0.6, \psi = 0.001, \delta = 0.01$ and $\phi = 0.2$. It is noticed that the film time T^* will increase/decrease in the presence of C in azimuthal/radial patterns as observed to the solid case. The permeability ψ is elaborated in Fig. 12. It is concluded that the squeeze time reduces due to rise of ψ compared to the solid case. Figures 13 and 14 represent the deviation of T^* w.r.t. h_m^* for distinct values of M_0 and l^*. According to these results, one concludes that there is a significant increase the time of approach by increase the effects of magnetization M and non-Newtonian lubricant l^*. The magnetic field applied sturdily opposes the flow in the film area and therefore considerable fluid quantity is preserved and the squeeze time increases. Figure 15 describes the variation of T^* against h_m^* for distinct values of β. Here, we found the decreasing trend of squeezing time for the higher values of β.
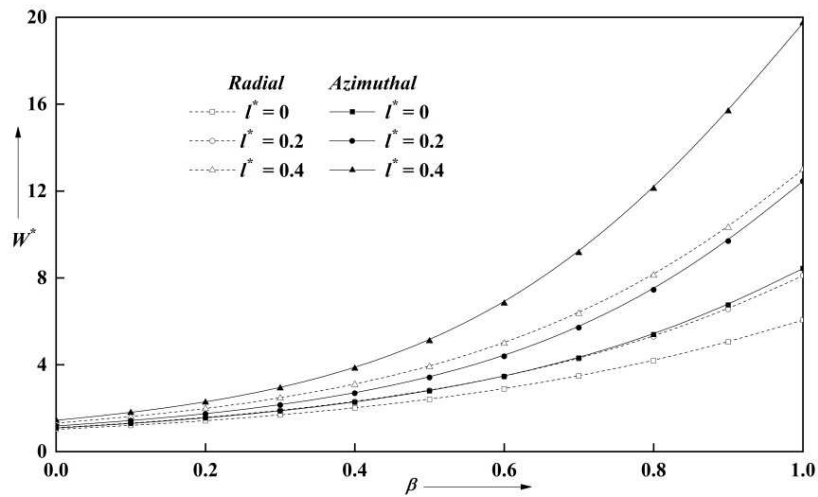
Fig. 10. Variation of non-dimensional load W^* with β for different values of l^* with $M = 2, m = 0.6, \psi = 0.001, \phi = 0.2, \delta = 0.01, C = 0.3.$
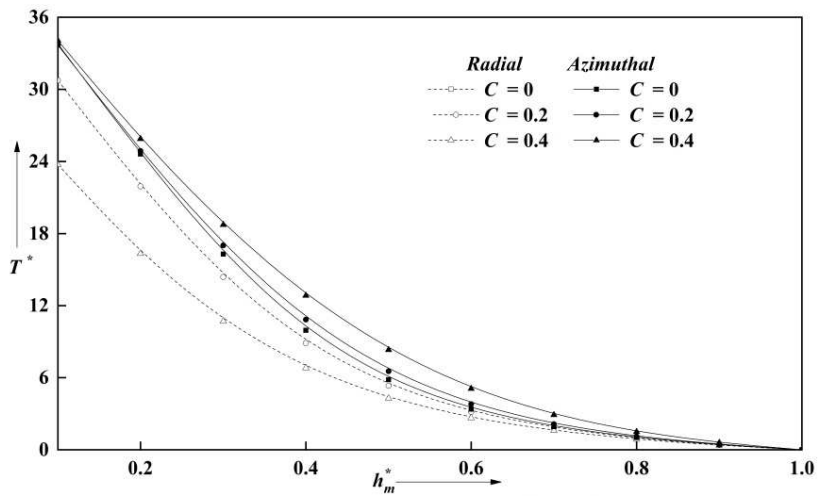

Fig. 11. Variation of non-dimensional squeeze film time T^* with h_m^* for different values of C with $M = 2, m = 0.6, \psi = 0.001, \phi = 0.2, \delta = 0.01, l^* = 0.3.$
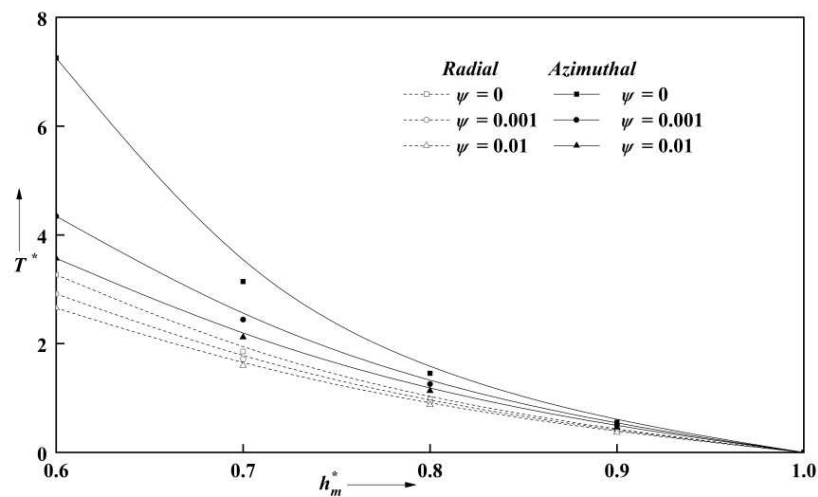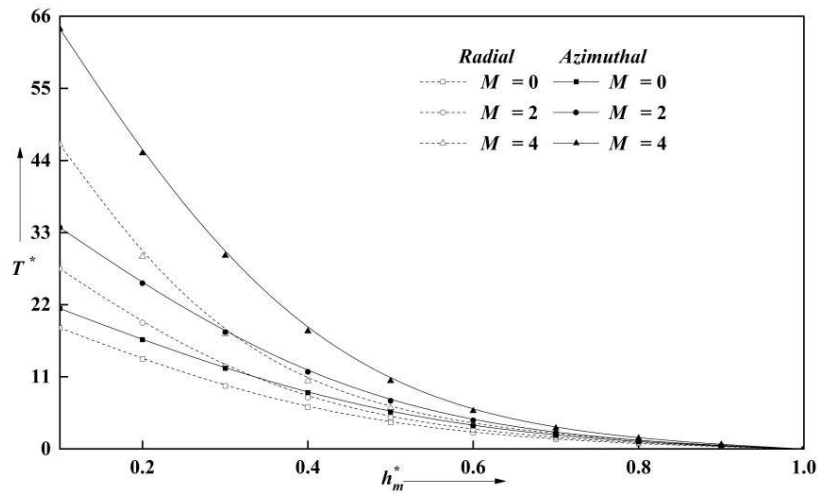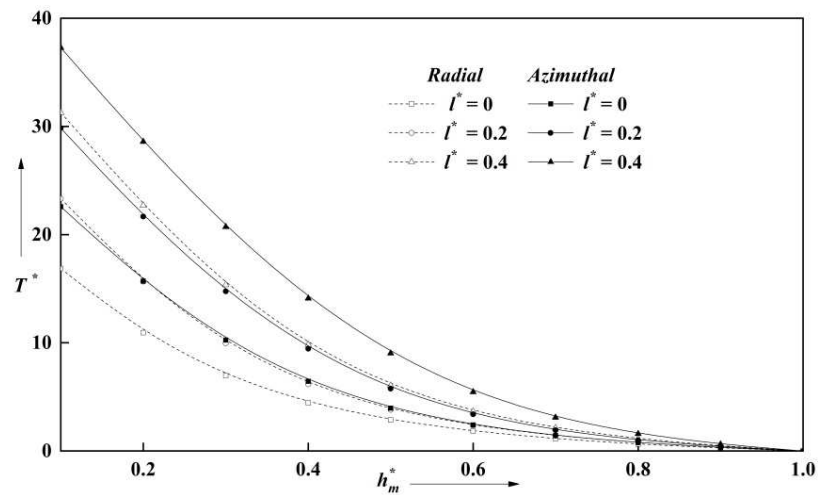

Fig. 12. Variation of non-dimensional squeeze film time T^* with h_m^* for different values of ψ with $M_0 = 2, m = 0.6, \beta = 0.5, \phi = 0.2, \delta = 0.01, l^* = 0.3, C = 0.3.$

Fig. 13. Variation of non-dimensional squeeze film time T^* with h_m^* for different values of M with $\psi = 0.001, m = 0.6, \beta = 0.5, \phi = 0.2, \delta = 0.01, l^* = 0.3, C = 0.3$.

Fig. 14. Variation of non-dimensional squeeze film time T^* with h_m^* for different values of l^* with $M_0 = 2, m = 0.6, \beta = 0.5, \phi = 0.2, \delta = 0.01, \psi = 0.001, C = 0.3$.
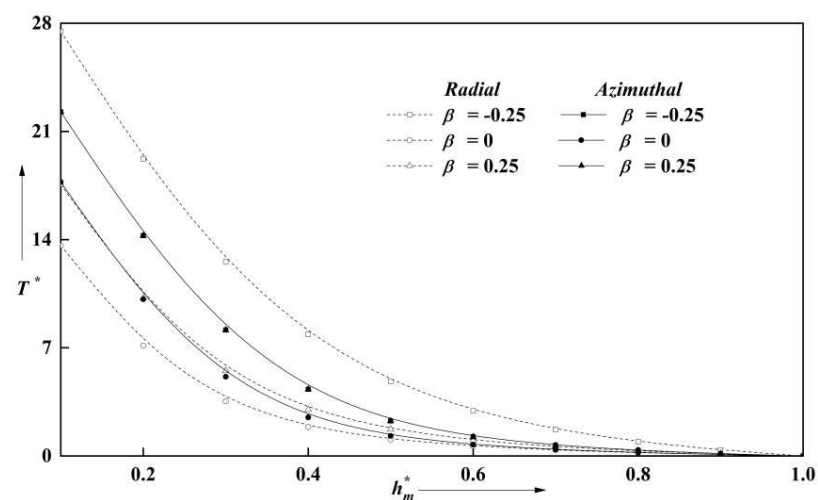

Fig. 15. Variation of non-dimensional squeeze film time T^* with h_m^* for different values of β with $M_0 = 2, m = 0.6, \psi = 0.001, \phi = 0.2, \delta = 0.01, l^* = 0.3, C = 0.3$.

4. Conclusion

Based on the stochastic theory of Christensen for irregular surfaces, the characteristics of MHD squeeze-film amid curved circular and flat plates with porosity and surface roughness showed the following conclusions:

1. For both patterns, i.e., the radial and azimuthal roughness, an improvement in the pressure, capability of load carrying and response time were noticed in the presence of transverse magnetic field which is applied externally and the couple stress lubricant.

2. The roughness regarding the surface affects the bearing characteristics. Due to the increase of surface roughness, huge load quantity is carried in the bearing and the squeeze-film response time extends in comparison to the smooth case.

3. In the limiting case, as $C \to 0$ and $\psi \to 0$, for one-dimensional curved circular and flat plates, the results for both roughness patterns can be reduced to the smooth surface and solid case.

4. The porous covering permeability reduces the characteristics of the squeeze film in comparison to the nonporous contention. As permeability raises the pressure distribution, the load carrying capability and response time are decreased.

Finally, we noticed from the results of Figs. 2 to 6 and also Figs. 11 to 15 that the squeeze film characteristics are continuously falling down for any increase of r^* and h_m^*. For better performance of the considered system, these values should be kept minimum. Furthermore, the reverse situation was found by increase the parameter β as shown in Figs. 7 to 10.

The characteristics of pressure distribution, load carrying capability and squeeze film time are boosted by educating the roughness parameter, Hartmann number, and couple stress lubricant, whereas they are lowered by raising the permeability, in contrast to the usual scenario. These physical quantities increase the bearing life and also propose suitable values to improve the working capacity of bearings.

Author Contributions

J. Jayaprakash identified and planned the topic for investigation and proposed the physical model; V. Govindan developed the mathematical modeling and examined the theory of validation. J. Patil carried out the solution procedure; B.N. Hanumagowda conducted the parametric analysis and interpretation of the results; H. Ahmad simulated the computational domain numerically; J.V. Tawade analyzed the numerical results. The manuscript was written with the contributions of all authors. All authors discussed the results, reviewed, and approved the final version of the manuscript.

Acknowledgments

Conflict of Interest

The authors declared no potential conflicts of interest concerning the research, authorship, and publication of this article.

Funding

Data Availability Statements

The datasets generated and/or analyzed during the current study are available from the corresponding author on reasonable request.

References

[1] Morgan, V.T., Porous Metal Bearings, *Powder Metallurgy*, 12(24), 1969, 426-451.

[2] Bujurke, N.M., Patel, H.P., Bhavi, S.G., Porous slider bearing with couple stress fluid, *Acta Mathematics*, 85, 1990, 99-113.

[3] Bhat, M.V., Hydrodynamic lubrication of an exponential porous slider bearing, *S.P. Uni. Res. J.*, 1, 1982, 93-96.

[4] Bhat, M.V., Daheri, G.M., Magnetic fluid based squeeze film in curved porous circular disks, *Journal of Magnetism and Magnetic Materials*, 127, 1993, 195.

[5] Rouleau, W.T., Hydrodynamic lubrication of narrow press-fitted porous metal bearings, *Transactions of the ASME. Series D, Journal of Basic Engineering*, 85, 1963, 123-128.

[6] Kashinath, B., Hanumagowda, B.N., MHD effect on Porous wide composite slider bearings lubricated with couple stress fluid, *Tribology Online*, 10(1), 2015, 11-20.

[7] Naduvinamani, N.B., Hiremath, P.S., Gurubasavaraj, G., Static and Dynamic behavior of squeeze film lubrication of narrow porous journal bearings with couple stress fluids, *Proceedings of the Institution of Mechanical Engineers, Part J: Journal of Engineering Tribology*, 45, 2001, 215.

[8] Bartz, W.J., Ether, J., Influence of Pressure viscosity oils on pressure, temperature and film thickness in elaso-hydrodynamically lubricated rolling contacts, *Proceedings of the Institution of Mechanical Engineers, Part C: Journal of Mechanical Engineering Science*, 222, 2008, 1271-1280.

[9] Biradar, T.V., Squeeze film lubrication between porous parallel stepped plates with couple stress fluids, *Tribology Online*, 8(5), 2013, 278-284.

[10] Srinivasacharya, D., Srinivasacharyalu, N., Odelu, O., Flow of Couple stress fluid between two parallel plates, *IAENG International Journal of Applied Mathematics*, 41(2), 2011, 2-10.

[11] Salma, A., Hanumegowda, B.N., Effect of MHD and viscosity variation on the couple stress squeeze film between curved circular and porous flat plate, *Partial Differential Equations in Applied Mathematics*, 6, 2022, 1-6.

[12] Kumar, V., Shah, V.A., Singh, S.J., Narwat, K., Sharma, S.C., Rotor-dynamic performance of porous hydrostatic thrust bearing operating under magnetic field, *Industrial Lubrication and Tribology*, 73(2), 2021, 350-357.

[13] Patil, S.M., Vinay, C.V., and P.A., D., Numerical approach to interpret the attributes of porous journal bearings using couple-stress fluid, *Industrial Lubrication and Tribology*, 73(2), 2021, 253-259.

[14] Naduvinamani, N.B., Rakesh, G., Double Layered porous Rayleigh step slider bearings lubricated with couple stress fluids, *Indian Journal of Science and Technology*, 15(28), 2022, 1389-1398.

[15] Kumar, S., Pai, N., Flow of Casson fluid through circular porous bearing, *CFD Letters*, 12(7), 2020, 48-56.

[16] Biplab, B., Prasun, C., Kishan, C., Theoretical investigation of porous hydrostatic journal bearings under micropolar fluid lubrication, *Proceedings of the Institution of Mechanical Engineers, Part N: Journal of Nanomaterials, Nanoengineering and Nanosystems*, 234, 2020, 12-18.

[17] Christensen, H., Some aspects of the functional influence of surface roughness in lubrication, *Wear*, 17(2), 1971, 149-162.

[18] Naduvinamani, N.B., Mareppa, R., Effect of surface roughness on magneto- hydrodynamic squeeze-film characteristics between a sphere and a porous plane surface, *Industrial Lubrication and Tribology*, 66(3), 2014, 365-372.

[19] Davies, M.G., The generation of pressure between rough fluids lubricated moving deformable surfaces, *Lubrication Engineering*, 102, 1963, 48-50.

[20] Prajapati, B.L., Behavior of squeeze film between rotating porous circular plate surface roughness and elastic deformation effects, *Pure and App. Math. Science*, 33, 1991, 27.

[21] Ting, L.L., Engagement behavior of lubricated porous annular disks part I, squeeze film phase-surface roughness and elastic deformation effects, *Wear*, 34, 1975, 159.

[22] Vadher, P.A., Vinodkumar, P.C., Patel, R.M., Behaviour of hydromagnetic squeeze films between two conducting rough porous circular plates, *Proceedings of the Institution of Mechanical Engineers, Part J: Journal of Engineering Tribology*, 222(4), 2008, 569-579.

[23] Rajshekar, M., Kashinath, B., Effect of surface roughness on MHD couple stress squeeze film characteristics between a sphere and a porous plane surface, *Advances in Tribology*, 2012, 2012, 935690.

[24] Masood, F.A., Elamparithi, S., Effect of surface roughness and MHD on Squeeze film characteristics for various finite porous plate geometry with couple stress fluid, *International Journal of Heat & Technology*, 41(3), 2023, 730.

[25] Adeshara, J.V., Sorathiya, S.G., Patel, H.P., Daheri, G.M., Patel, R.M., Surface roughness and deformation effect on the performance of the hydromagnetic fluid based squeeze film on rough porous truncated conical bearing, *Journal of Mechanical Engineering and Research*, 46(1), 2023, 1-18.

[26] Rahul, A.K., Rao, P.S., Rabinowitsch fluid flow with viscosity variation application of porous-rough circular stepped plate, *Tribology International*, 154, 2021, 106635.

[27] Hanumagowda, B.N., Lubrication of Squeeze Film Between Porous Rough Circular Plates with Rabinowitsch Fluid Model, *Tuijin Jishu/Journal of Propulsion Technology*, 44(4), 2023, 6284-6294.

[28] Salma, A., Hanumagowda, B.N., Sreekala, C.K., Muhammad, T., Insight into the dynamics of couple-stress fluid through the porous medium between a curved circular plate and a rough flat plate: comparative analysis between radial and azimuthal roughness, *Chinese Journal of Physics*, 88, 2024, 991-1009.

Appendix A

$$g_{11} = \frac{A^2}{\left(A^2 - B^2\right)}\left(\frac{\cosh\left\{B(2z-h)/2l\right\}}{\cosh\left(Bh/2l\right)}\right) \tag{A1}$$

$$g_{12} = \frac{B^2}{\left(A^2 - B^2\right)}\left(\frac{\cosh\left\{A(2z-h)/2l\right\}}{\cosh\left(Ah/2l\right)}\right) \tag{A2}$$

$$A = \left\{\frac{1 + \left(1 - 4M^2l^2/h_m^2\right)^{\frac{1}{2}}}{2}\right\}^{\frac{1}{2}}, \ B = \left\{\frac{1 - \left(1 - 4M^2l^2/h_m^2\right)^{\frac{1}{2}}}{2}\right\}^{\frac{1}{2}} \tag{A3}$$

$$g_{21} = \frac{2\cosh\left\{(z-h)/\sqrt{2l}\right\} + 2\cosh\left(z/\sqrt{2l}\right)}{2\left\{\cosh\left(h/\sqrt{2l}\right) + 1\right\}} \tag{A4}$$

$$g_{22} = \frac{\left(z/\sqrt{2l}\right)\sinh\left\{(z-h)/\sqrt{2l}\right\} + \left\{(z-h)/\sqrt{2l}\right\}\sinh\left(z/\sqrt{2l}\right)}{2\left\{\cosh\left(h/\sqrt{2l}\right) + 1\right\}} \tag{A5}$$

$$g_{31} = \frac{\cos B_2 z\cosh A_2(z-h) + \cosh A_2 z\cosh B_2(z-h)}{\cosh A_2 h + \cosh B_2 h} \tag{A6}$$

$$g_{32} = \frac{\cot\theta\left\{\sinh A_2 z\sinh B_2(z-h) + \sin B_2 z\sinh A_2(z-h)\right\}}{\cosh A_2 h + \cosh B_2 h} \tag{A7}$$

$$A_2 = \sqrt{M/lh_m}\cos(\theta/2), \ B_2 = \sqrt{M/lh_m}\sin(\theta/2), \ \theta = \tan^{-1}\left(\sqrt{4l^2M^2/h_m^2 - 1}\right) \tag{A8}$$

ORCID iD

J. Jayaprakash https://orcid.org/0009-0000-9720-2538
Vediyappan Govindan https://orcid.org/0000-0003-4750-1964
Jagadish Patil https://orcid.org/0000-0001-8000-3962
Bannihalli N. Hanumagowda https://orcid.org/0000-0002-1210-0231
Hijaz Ahmad https://orcid.org/0000-0002-5438-5407
Jagadish V. Tawade https://orcid.org/0000-0003-2070-1763

Publisher's Note Shahid Chamran University of Ahvaz remains neutral with regard to jurisdictional claims in published maps and institutional affiliations.